Database-driven Safe Flight Envelope Protection for Impaired Aircraft

Zhang, Ye; Huang, Yingzhi; Chu, Q. P.; de Visser, Coen

DOI
10.2514/6.2020-1374

Publication date
2020

Document Version
Final published version

Published in
AIAA Scitech 2020 Forum

AIAA SciTech Forum
6-10 January 2020, Orlando, FL
AIAA Scitech 2020 Forum

10.2514/6.2020-1374

Database-driven Safe Flight Envelope Protection for Impaired Aircraft

Ye Zhang*, Yingzhi Huang†, Qiping Chu‡, and Coen C. de Visser§
Delft University of Technology, Delft, 2629HS, The Netherlands.

In this paper, an online flight envelope protection system is developed and implemented on impaired aircraft with structural damage. The whole protection system is designed to be a closed-loop of several sub-systems, including system identification, damage classification, flight-envelope prediction and fault-tolerant control. Based on the information given by damage classification, the flight envelopes are explicitly retrieved and processed online from the database and fed into the fault-tolerant controller, which makes the protection system adaptive to a wide range of abnormal conditions. Simulation results show that with envelope protection, loss-of-control accidents are more likely to be prevented, since both the controller and pilots are aware of the shrunken flight envelopes after damage and excessive commands are restricted. In this way, the fault-tolerance of the impaired aircraft can be effectively enhanced.

I. Introduction

Loss-of-control (LOC) prevention by means of flight envelope protection has seen much attention recently. Currently, most modern commercial and military are equipped with some form of flight envelope protection systems, which prevent violations of pre-defined constraints on flight states such as speed, angle of attack, bank angle and load factor. The function of a flight envelope protection system is two-fold: an augmentation of the flight controller to monitor and maintain the aircraft within its flight envelope [1–4], and an auxiliary system to inform pilots of the current flight envelopes via human-machine interaction mechanisms such as haptics and visual displays [5–8]. The first function prevents pilots from over-steering the aircraft by limiting the commands to the flight controller, and the second function provides information so that pilots can decide on appropriate control strategies without violating the envelope boundaries. These two functions work in cooperation to enhance the flight safety.

One problem with current-day flight envelope protection systems is that they work with static flight envelopes, under the assumption that the intrinsic aircraft flight dynamics do not change under any circumstances. When abnormal cases like structural damage and icing occur, however, the performance of the aircraft may suddenly or slowly degrade, which is ultimately reflected in a change of the flight envelope [9, 10]. If the new, in most cases reduced flight envelopes are not provided to the control system or pilots in time, the aircraft might unintentionally leave the safe region, a situation that may evolve into an LOC event.

An online flight envelope prediction system developed in our previous research [10, 11] addressed this problem by building a database of various key abnormal cases with their associated changed flight envelopes. The proposed system considerably reduces the computational burden and circumvents many complications related to online flight envelope prediction.

As a follow-up of our previous research, this paper implements an online flight envelope protection system to protect the aircraft from LOC situations where the flight envelopes have suddenly changed in-flight. The system is designed to improve responses to potential LOC scenarios by efficiently processing and retrieving data online. Unlike open-loop configurations discussed in previous papers, the proposed envelope protection system functions in closed-loop, combining system identification, learning-based diagnosis, database-driven envelope prediction and fault tolerant control. The advantage of this modular design is that only envelopes that are explicitly referred to by the system need to be retrieved from the database, and the re-design of the overall protection and control system is not necessarily needed

*PhD Student, Control and Simulation Section, Faculty of Aerospace Engineering, Delft University of Technology; Kluyverweg 1, 2629HS, Delft, The Netherlands. AIAA Student Member

†PhD Student, Control and Simulation Section, Faculty of Aerospace Engineering, Delft University of Technology; Kluyverweg 1, 2629HS, Delft, The Netherlands. AIAA Member

‡Associate Professor, Control and Simulation Section, Faculty of Aerospace Engineering, Delft University of Technology; Kluyverweg 1, 2629HS, Delft, The Netherlands. AIAA Member

§Assistant Professor, Control and Simulation Section, Faculty of Aerospace Engineering, Delft University of Technology; Kluyverweg 1, 2629HS, Delft, The Netherlands. AIAA Member

[11]. Being connected to a scalable database, resiliency can be achieved in various abnormal situations that can be modeled a priori.

The primary contribution of this work is the integration of different modules that were separately developed in previous papers. This paper also contributes to a procedure to generate a safe level of excitation inputs for system identification in abnormal situations, which aims to achieve a balance between safety and accuracy. A final contribution of this paper is the first-time application of envelope protection in structural-damage scenarios, which are rare but dangerous cases. Offline analysis and online simulations enable models and envelopes in the database to be fully validated and verified for structural-damage cases. The simulations are conducted in near real-time, which shows the feasibility of onboard applications of the proposed system.

II. Online Implementation

Sudden occurrence of abnormal cases, like structural damage and system failures, may cause an abrupt change to the flight dynamics as well as control authority, leading to a potential loss of stability and control [9, 10]. In such cases, fast responses and high-frequency control inputs for new control strategies are required, which are difficult or even physically impossible for human pilots to achieve. Instead, an automatic fault tolerant controller (FTC) can be reconfigured to regain control of the aircraft given the knowledge of the new flight envelope. Therefore, this research focuses on the first function of the flight envelope protection system, which uses prediction of the new flight envelope to reconfigure the FTC.

The implementation of a flight envelope prediction system, which includes system identification, fault/damage diagnosis and database building has been thoroughly discussed in [10, 11]. However, none of these have practical meaning if they are not connected and running in-the-loop with an FTC. Figure 1 shows the complete flight envelope protection system, which combines previously developed modules of envelope prediction, together with an FTC. In this way, commands from pilot/autopilot as well as flight states can be constrained within the new flight envelope in abnormal situations.

There is a whole spectrum of abnormal situations, from "benign" to "immediately catastrophic". The most extreme case indicates the situation where the remaining flight envelope is too small for aircraft to recover from upset conditions and perform maneuvers. For example, under total loss of actuators and strong gust wind, the aircraft may immediately enter a LOC condition without any effective control. Therefore, discussions on catastrophically impaired aircraft are excluded from the scope of this paper.

What we are focusing on are less extreme but still "potentially" catastrophic situations, where LOC is likely to happen if maneuvers are initiated without knowledge of the current abnormal condition and reduced flight envelopes. In these cases, it is still possible to control the aircraft given sufficient control authority and maneuverability based on the updated flight envelope. The protection system proposed in this paper thus plays an important role in preventing impaired aircraft from entering LOC conditions after a sudden change in the system dynamics and control authorities, and turning them into survivable incidents.

The flight after faults/damage can be divided into two phases. During the first phase, the initial trim condition is disturbed by sudden faults/damage and the aircraft is quickly re-stabilized by the onboard fault tolerant controller and actuators. Meanwhile, the detection alarm is triggered, which starts the re-identification of the aerodynamic model. During the re-identification process, small actuator commands are generated and measured, which are used as the excitation inputs for the identification of control effectiveness. Triggered by the detection alarm, the covariance matrix is reset to its initial value so that the re-identification is mostly influenced by new data in the changed situation. Once the identification errors and covariance matrix converge to sufficiently small values, the identified aerodynamic coefficients converge to their new values, which are used for the fault and damage diagnosis system. In this way, the system identification and diagnosis system provides information on the current abnormal situation of the aircraft as well as the reduced control authorities, which generate a match with a case index to one flight envelope in the database.

The second phase starts when the aircraft has to maneuver (e.g. turning, ascend, descend). This phase is more safety-critical, since the maneuver may cause incremental forces and moments that are beyond the current control authority and potentially lead to LOC. Therefore, during phase 2, it is extremely important to consider the remaining control authority and the boundary of the new reduced flight envelope when giving commands to the controller.

As illustrated in Fig. 1, half of the loop on the right is more active during phase 1, where the re-stabilization and diagnosis of the impaired aircraft is achieved. The left side of the loop is more important during phase 2, where flight envelope prediction and protection are connected to ensure that the maneuver is always kept within the updated safe flight envelope. The detailed descriptions of these two phases are given in the next subsections.

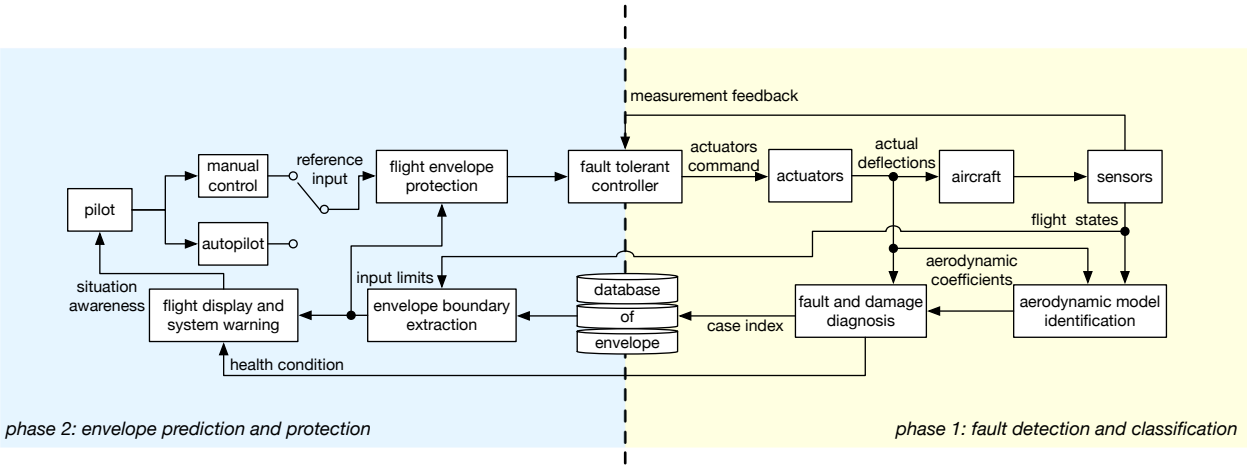

Fig. 1 An overview of the complete loop to be implemented online

A. Phase 1: From Damage to Trim

When an unexpected failure, such as structural damage, suddenly occurs, a passive FTC is used to allocate the actuators to re-stabilize the aircraft. The advantage of the passive FTC is that it responds faster to abnormal situations than human pilots. Hence, in phase 1, the mitigation of unexpected failures is quickly achieved by the FTC if sufficient control authority is available. The quick reaction of the controller alleviates the work load of pilots so that they can focus more on situational analysis and higher-level decision-makings.

In case of vertical tail loss, for example, when it is hardly possible to maintain directional stability via rudder, alternate control methods like differential thrust and combined use of ailerons can be applied automatically by the FTC [12]. A more frequently occurring case is engine failure, which imposes a sudden asymmetric side force and a non-zero side-slip angle (β) followed by a roll motion. Under such emergencies, with the help of an automatic FTC, rudder deflection is used to mitigate the adverse yaw and maintain a zero β.

The availability of persistent excitation inputs is one of the key issues in system identification. In abnormal situations, aircraft is more likely to lose control during maneuvering. Hence, excitation inputs, if required, should be given with safety considerations. However, a significant challenge is to decide the scale of identification inputs before diagnosis information is provided. In most literature, excitation inputs are given based on pilot experience and intuitions, which in the case of failures can pose a large potential risk. In this paper, we propose to quantify the scale of excitation inputs by first retrieving the most conservative flight envelope in the database, and then adding incremental inputs when more diagnosis information flows in. The retrieved flight envelope is used to determine how small the inputs should be in order to reduce the risk of LOC.

One issue with this constrained excitation is that limited inputs may give inaccurate identification results. The lack of accuracy can be compensated for by the high generalization ability of well-trained classifiers used in the diagnosis system [10]. In this way, priority can be given to safety while the fidelity of diagnosis can be maintained, even when model identification is compromised.

The diagnosis system is composed of several parallel classifiers, each of which corresponds to one of the pre-defined damage and fault locations. The classification is based on the learning results that are trained offline and stored in the system, and each classifier has different aerodynamic coefficients as its inputs. Based on the outputs of all the classifiers, the decision-making process determines the type, location and severity of current faults and damage.

The classification and decision-making results will then generate the case index to retrieve the corresponding flight envelopes in the database. If the diagnosis system indicates that there are multiple damage locations, or there is a necessity for flight envelope interpolation, more than one flight envelope will be retrieved from the database. More details on the database approach can be found in our previous papers [10, 11].

B. Phase 2: From Trim to Maneuver

In the second phase the stabilized aircraft will attempt to conduct larger amplitude maneuvers (e.g. turning, ascending, descending), and active control strategies can be applied. However, during this phase, LOC can be caused

by overly aggressive commands. In an icing scenario simulated in [13], even though ice accretion itself did not initiate immediate LOC, the safe flight envelope had greatly changed. When the protection system failed to take these changes into account, a combined pitch up and roll maneuver after icing easily commanded the aircraft over its envelope limits and caused a LOC accident.

Similarly, the faults and damage to aerodynamic surfaces and actuators always lead to reduced stability margin and control authority. If the aircraft is subjected to incremental moments due to asymmetric damage and faults, it will cause further reduction of available control power during the maneuver. All these changes are reflected in the reduced flight envelopes. If the maneuver command is given without considering the changed envelopes, the aircraft may fly into unrecoverable states. In some cases, for instance, excessive inputs may generate incremental moments that cannot be counteracted given the remaining control authorities, leading to the saturation of actuators and LOC. Therefore, flight envelopes retrieved from the database are incorporated in the control and warning system to protect the aircraft from LOC situations. In this way, within the remaining maneuverability, the envelope protection system can help the pilots safely maneuver and eventually land the aircraft after sudden damage.

III. Reconfiguration of Flight Controls

An FTC is designed to reconfigure the flight control laws when there are system faults and damage. The reconfigured controller is expected to achieve the control objective and satisfactory performance by using remaining control authorities to adapt to the changed system dynamics and mitigate the adverse impact of faults and damage. A comprehensive review of FTCs and their comparisons can be found in [14, 15].

Among various adaptive fault tolerant control methods for nonlinear systems, the incremental nonlinear dynamic inversion (INDI) control [16, 17] has been intensively applied to different types of aircraft. The INDI method can be considered as an incremental form of the widely used feedback linearization approach [18, 19]. The advantage of the INDI method is that it makes the controller significantly less sensitive to model mismatch with simpler control design. In situations of system faults, failures and especially structural damage, the presence of model mismatch is inevitable. The INDI method uses sensor information to replace a large part of the model including its un-modeled uncertainties, making it much less model-dependent and very suitable for fault tolerant control. In practice, the high performance and adaptiveness of the INDI controller has been proved by many published results from simulations as well as real-world flight tests. In [17], a flight control strategy based on the INDI method has been applied to a T-tailed UAV simulation model, which showed increased robustness of the system. Real-world flight tests on a quad-rotor UAV have demonstrated high performances of the INDI controller with very coarse knowledge of model parameters in advance [20, 21]. Highly nonlinear and inherently unstable models of helicopters [22] as well as over-actuated tailless aircraft [23] also utilized the INDI method in controller design to achieve efficient tracking of the commands under model uncertainties. In [24], INDI was applied to a multi-loop fashion for trajectory control of a Cessna Citation aircraft in a simulation environment. Most significantly, real flight tests have been successfully conducted on a Cessna Citation II aircraft [25]. In these flight tests, the INDI control method was integrated with the fly-by-wire and sensor systems, and performed with satisfying results and robustness to a large amount of model mismatch [25].

In this paper, when the flight envelope limits are retrieved, the flight envelop protection can be implemented through the INDI flight controller to ensure that the aircraft stays within the state boundaries. By applying the command limiting strategy [4], the envelope limits can be mapped onto command limits that are enforced into the controller.

The aircraft is controlled in a multi-loop structure based on its dynamics model. In abnormal situations, maintaining control of attitude and aerodynamic angles is the primary concern. As illustrated in Fig. 2, the control system consists of two loops: an outer loop for control of the roll angle ϕ, angle of attack α, and side-slip angle β; an inner loop for the angular rates $\boldsymbol{\omega} = [p, q, r]^T$ corresponding to roll, pitch and yaw respectively. The engine throttle is controlled by a separated auto-throttle loop to maintain a commanded velocity. The commands for $[\phi, \alpha, \beta, V]^T$ are given by the pilots/autopilots. The dynamics of $[\phi, \alpha, \beta]^T$ can be written in the form:

$$\begin{bmatrix} \dot{\phi} \\ \dot{\alpha} \\ \dot{\beta} \end{bmatrix} = F_{out} + G_{out}\,\boldsymbol{\omega} = \begin{bmatrix} 0 \\ f_\alpha \\ f_\beta \end{bmatrix} + \begin{bmatrix} 1 & \sin\phi\tan\theta & \cos\phi\tan\theta \\ \dfrac{-uv}{\sqrt{u^2+w^2}} & 1 & \dfrac{-vw}{\sqrt{u^2+w^2}} \\ \dfrac{w}{\sqrt{u^2+w^2}} & 0 & -\dfrac{u}{\sqrt{u^2+w^2}} \end{bmatrix} \begin{bmatrix} p \\ q \\ r \end{bmatrix} \tag{1}$$

where,

$$f_\beta = \frac{1}{\sqrt{u^2+w^2}}\left[-\frac{uv}{V^2}(A_x - g\sin\theta) + (1-\frac{v}{V^2})(A_y + g\sin\phi\cos\theta) - \frac{vw}{V^2}(A_z + g\cos\phi\cos\theta)\right] \tag{2}$$

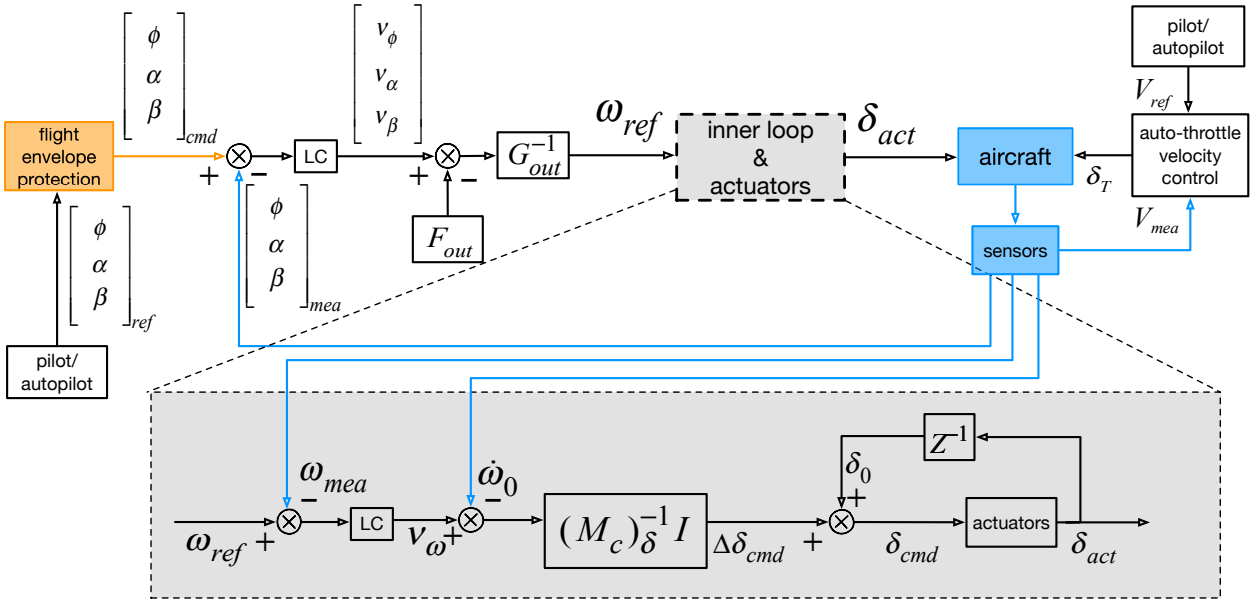

Fig. 2 A multi-loop NDI/INDI control structure; LC indicates a Linear Controller

$$f_\alpha = \frac{1}{u^2 + w^2}\left[u(A_z + g\cos\phi\cos\theta) - w(A_x - g\sin\theta)\right] \tag{3}$$

and A_x, A_y, A_z denotes the specific forces along the body X/Y/Z axis; u, v, w are the velocity components along the body X/Y/Z axis. The values of these states as well as the Euler angles are measured from onboard sensors.

Since Eq. 1 and 2 contains no model uncertainty, a classic NDI controller is applied to the outer loop. The desired input to the inner-loop control $\boldsymbol{\omega}_{ref} = [p, q, r]^T_{ref}$ is solved by introducing a virtual input vector $[\nu_\phi, \nu_\alpha, \nu_\beta]^T$ to the outer-loop controller:

$$\boldsymbol{\omega}_{ref} = G^{-1}_{out}\left(\left[\nu_\phi, \nu_\alpha, \nu_\beta\right]^T - F_{out}\right) \tag{4}$$

substituting Eq. 4 into the dynamics equation Eq. 1 yields a decoupled linear relation:

$$\left[\dot{\phi}, \dot{\alpha}, \dot{\beta}\right]^T = \left[\nu_\phi, \nu_\alpha, \nu_\beta\right]^T \tag{5}$$

Therefore, the virtual input $\left[\nu_\phi, \nu_\alpha, \nu_\beta\right]^T$ can be solved by a linear controller (LC), as shown in Fig. 2.

The resulting $\boldsymbol{\omega}_{ref}$ is used for controlling the inner-loop of angular rates, where the Euler equations of motion are used [17]:

$$\mathbf{M} = \mathbf{I}\dot{\boldsymbol{\omega}} + \boldsymbol{\omega} \times \mathbf{I}\boldsymbol{\omega} \tag{6}$$

where $\mathbf{M} = [L, M, N]^T$ are the angular moments acting on the aircraft, and the inertia matrix is denoted by $\mathbf{I}$.

The moments $\mathbf{M}$ can be specified as a combination of flight-states-related moments $\mathbf{M}_a$ generated by airframe aerodynamics, and actuator-related moments $\mathbf{M}_c$ generated by the control surface deflections. Solving the above equation for $\dot{\boldsymbol{\omega}}$ yields [17]:

$$\dot{\boldsymbol{\omega}} = \mathbf{I}^{-1}(\mathbf{M}_a + \mathbf{M}_c - \boldsymbol{\omega} \times \mathbf{I}\boldsymbol{\omega}) \tag{7}$$

by assuming on the linear relation between $\mathbf{M}_c$ and actuator deflections $\boldsymbol{\delta} = [\delta_a, \delta_e, \delta_r]^T$, which is:

$$\mathbf{M}_c = (\mathbf{M}_c)_\delta\, \boldsymbol{\delta} = \frac{1}{2}\rho V^2 S \begin{bmatrix} bC_{l_{\delta_a}} & 0 & bC_{l_{\delta_r}} \\ 0 & \bar{c}C_{m_{\delta_e}} & 0 \\ bC_{n_{\delta_a}} & 0 & bC_{n_{\delta_r}} \end{bmatrix} \begin{bmatrix} \delta_a \\ \delta_e \\ \delta_r \end{bmatrix} \tag{8}$$

where $(\mathbf{M}_c)_\delta = \dfrac{\partial}{\partial \delta}\mathbf{M}_c$. If NDI is applied to the inner-loop, the actuator deflections $\boldsymbol{\delta}$ can be solved by introducing a virtual input $\boldsymbol{\nu}_\omega$ to the inner-loop, which yields:

$$\boldsymbol{\delta} = \mathbf{M}_c^{-1}\left(\mathbf{I}\boldsymbol{\nu}_\omega + \boldsymbol{\omega} \times \mathbf{I}\boldsymbol{\omega} - \mathbf{M}_a\right) \tag{9}$$

Similar to the outer-loop, the introduction of a virtual input vector $\boldsymbol{\nu}_\omega$ yields a linear system $\dot{\boldsymbol{\omega}} = \boldsymbol{\nu}_\omega$, of which a linear controller is used to generate $\boldsymbol{\nu}_\omega$ depending on the errors between the measured and desired value of $\boldsymbol{\omega}$, as shown in Fig. 2.

It is noticed in Eq. 9 that the control law depends on the full aerodynamic model of $\mathbf{M}_a$ and $\mathbf{M}_c$. However, due to the occurrence of damage, a lot of uncertainties are introduced to the aerodynamic model. Hence, the mismatch of the estimated $\mathbf{M}_a$ will have an undesired impact on the performance of the NDI controller. Alternatively, the INDI method is used for inner loop to fix this issue. Consider only computing the increments of actuator deflections at each execution, which are only influenced by $\mathbf{M}_c$, a large part of model uncertainties can be mitigated. The incremental part is obtained by a first-order Taylor approximation of $\dot{\boldsymbol{\omega}}$ in Eq. 7[17]:

$$\dot{\boldsymbol{\omega}} \approx \dot{\boldsymbol{\omega}}_0 + \frac{\partial}{\partial \boldsymbol{\omega}} \left[\mathbf{I}^{-1}(\mathbf{M}_a - \boldsymbol{\omega} \times \mathbf{I}\boldsymbol{\omega})\right]_{\boldsymbol{\omega}_0, \boldsymbol{\delta}_0} (\boldsymbol{\omega} - \boldsymbol{\omega}_0) + \frac{\partial}{\partial \boldsymbol{\delta}} \left[\mathbf{I}^{-1}\mathbf{M}_c\right]_{\boldsymbol{\omega}_0, \boldsymbol{\delta}_0} (\boldsymbol{\delta} - \boldsymbol{\delta}_0) \tag{10}$$

where $\boldsymbol{\omega}_0$ and $\boldsymbol{\delta}_0$ are the measured values of the previous time step. For small time increments, the change rate of angular rate $(\boldsymbol{\omega} - \boldsymbol{\omega}_0)$ is considered to be negligible compared to the change of actuator deflection. Hence, by denoting $(\boldsymbol{\delta} - \boldsymbol{\delta}_0)$ as $\Delta\boldsymbol{\delta}$, Eq. 10 can be simplified as:

$$\dot{\boldsymbol{\omega}} \approx \dot{\boldsymbol{\omega}}_0 + \left[\mathbf{I}^{-1}(\mathbf{M}_c)_\delta\right] \Delta\boldsymbol{\delta} \tag{11}$$

where $(\mathbf{M}_c)_\delta = \frac{\partial \mathbf{M}_c}{\partial \delta}$ .It can be observed that a large part of the aerodynamic model $\mathbf{M}_a$ is canceled since only the incremental form is considered. On the assumption of accurate sensor information of angular accelerations, the commanded incremental deflections of actuators can be solved by:

$$\Delta\boldsymbol{\delta}_{cmd} = (\mathbf{M}_c)_\delta^{-1}\mathbf{I}(\boldsymbol{\nu}_\omega - \dot{\boldsymbol{\omega}}_0) \tag{12}$$

which yields the commanded control input to the aircraft:

$$\boldsymbol{\delta}_{cmd} = \boldsymbol{\delta}_0 + \Delta\boldsymbol{\delta}_{cmd} \tag{13}$$

It should be noted that the derivation of the INDI method requires actuators with fast deflection responses, so the performance of the controlled may be degraded when the actuator saturated due to system faults or aircraft damage, which will be discussed later in this paper.

IV. Case Study and Simulation Results

In this section, an online simulation of the complete envelope prediction and protection system (see Fig. 1) is conducted to investigate its online feasibility in given scenarios. The simulation is based on a model of the Cessna Citation aircraft, which is a twin-jet business aircraft shown in Fig. 3. The aircraft model is incorporated in a high-fidelity simulation environment in Matlab Simulink for developing and testing new methodologies in a fly-by-wire system before they are implemented in real flight [26]. The simulation environment is called "DASMAT", which is the abbreviation of "Delft University Aircraft Simulation Model and Analysis Tool". The Cessna Citation aircraft model and DASMAT have been used in our previous papers on flight envelope calculation, damage modeling and classification [10, 11]. In this paper, databases of flight envelopes [11] are built in the form of look-up tables and incorporated in the DASMAT.

In order to demonstrate the importance of envelope protection, two structural-damage cases are modeled in DASMAT. As shown in Fig. 3, the first case is symmetrical damage to the rudder, and the second case is asymmetrical damage to the left wing and aileron. The combination of both wing and rudder damage is also simulated and discussed. Due to the coupling between roll and yaw motions, the loss of directional control will generate a rolling moment that may lead to the loss of lateral control if the available control power is exceeded. Figure 4 shows the flight envelopes retrieved from the database, which are used for online envelope update and protection. Obvious shrinkage of envelopes after each damage case can be observed in Fig. 4, which shows the influence of structural damage on the maneuverability of the impaired aircraft.

The simulations are performed in DASMAT under normal and abnormal flight conditions. During each simulated flight, the aircraft is initially trimmed at $100m/s$ and $5000m$ with $\alpha = 3.7°$. Sensor faults and failures are not considered in this paper, so all sensors are assumed to function normally. In each simulation, the flight lasts 50 seconds, which costs around 160 seconds in real time on a laptop with 4GB RAM and an update rate of 100Hz. According to the Matlab profiler, in the total recorded time of 160 seconds, nearly 130 seconds are spent on numerical calculations of

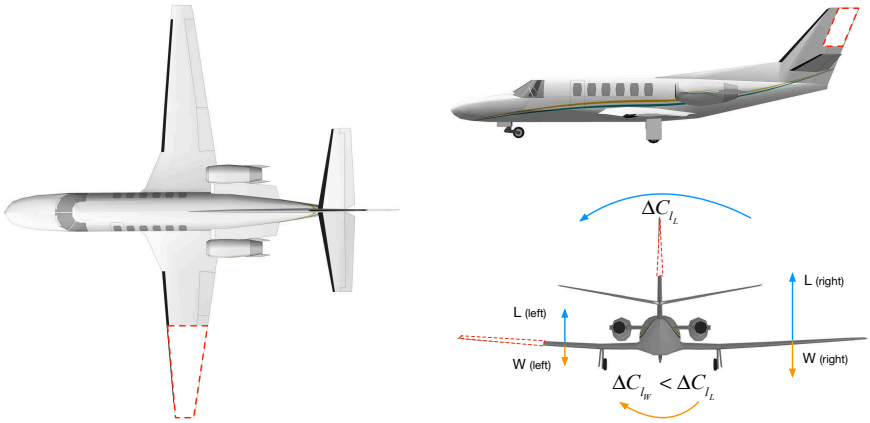

Fig. 3 A three-view illustration of a damaged Cessna Citation aircraft

the aircraft responses from the complex aircraft model in the Simulink. If some flight states can be directly measured instead of computed, as in real flight, nearly 80% of the computation time can be saved. Compared to the aircraft model, the computational burden of system identification, damage classification, database retrieval and fault tolerant control used in the envelope protection system is trivial, which indicates that the proposed system is feasible for online application. Besides, the time efficiency of the simulation can be further improved by optimizing the Matlab codes or transplanting them into C/C++ for real-time implementations.

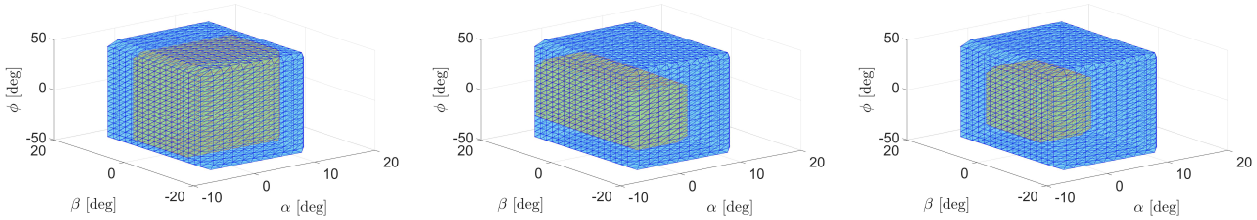

(a) 50% tip loss of rudder (b) 50% tip loss of left wing (c) Combined damage of rudder and wing

Fig. 4 Normal flight envelopes (blue) and their reduced forms after structural damage (yellow) retrieved from the database

A. Rudder Damage

The rudder is commonly used to maintain zero sideslip angle under side force and adverse yaw moments, and to align the aircraft with the runway for crosswind landing. When aileron control is limited, rudder can also be used as an alternative control effector for turning the aircraft [12]. In such a situation, a certain (non-zero) sideslip angle is given as the reference input by the pilot/autopilot.

When the rudder is damaged, in order to maintain the same value of β, more rudder deflections are required compared to a normal situation. If the reference input β is given without considering the reduced control effectiveness, the damaged rudder may soon saturate and lead to the loss of directional control. The aim of β-protection is to prevent such aggressive use of the rudder.

As discussed in the previous section, the re-identification and classification form the primary phase of envelope prediction and protection. The re-identification is triggered when the errors between measured and modeled outputs exceed a certain threshold. The triggering threshold is pre-defined based on the lowest damage scale modeled in the simulation. For asymmetrical damage (e.g., wing damage), the re-identification signal is normally induced by unequal forces and increments of moments.

Rudder damage, however, is symmetrical, which does not induce constant increments of yawing moment, unless it is combined with rudder hard-over or asymmetric engine failures. Nevertheless, it is still possible to detect the errors if the damaged rudder deflects to, for instance, maintain a non-zero β command. Additionally, reports on past flight

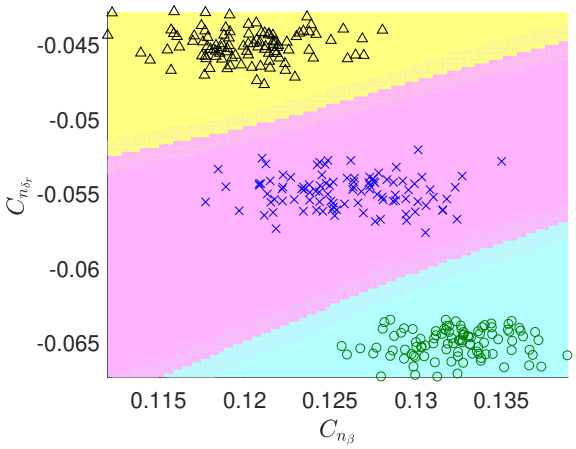

Fig. 5 Training result of rudder damage using neural networks (damage levels ◯ : 30% × : 40% Δ : 50%)

accidents reveal that rudder and vertical tail damage is often accompanied, or induced by sudden external disturbances and turbulence, when the rudder deflects to re-trim the aircraft.

For the online identification process, the recursive least squares (RLS) method has been implemented [11, 18]. At each time instant, the covariance matrix gives some information of the reliability of the re-identified model parameters, which is closely related to the sufficiency of each state input. In abnormal situations, recovering and re-stabilizing maneuvers only excite a limited range of states, resulting in an updated local model of the current flight condition. By observing the variance of each estimated parameter, it is found that not all parameters are identifiable. Nevertheless, the advantage of using classification is that it does not require all changed parameters to be accurately re-estimated but only parameters that quickly converge are selected as classification features. This advantage naturally circumvents the safety concerns associated with obtaining global models in abnormal situations.

The classification is based on the neural-network (NN) method discussed in [10]. Two parameters, C_{n_β} and $C_{n_{\delta_r}}$, are selected as the classification features. They can either be trained as two individual features, which yields two separate classifiers, or as a feature set of one classifier. The advantage of using NN classification is that multiple classes can be trained in one classifier of the same classification features. Figure 5 shows the training result of three rudder-damage levels, which is quantified by % of tip loss.

Each data point for training, denoted by different markers in Fig. 5, is generated by system identification from each individual simulation test. The variance of training data in each class is caused by the variance in the level of external noise, the initial flight conditions and the sufficiency of excitation inputs given in every simulation. It can be observed that the variance of C_{n_β} is larger than that of $C_{n_{\delta_r}}$, implying that the identification of $C_{n_{\delta_r}}$ is more sufficiently excited. Based on this training set, the classifier is more tolerant of the imprecise identification of C_{n_β} due to possible lack of sufficient excitation after damage.

In this section, a 50% tip loss of the rudder is simulated by changing the values of aerodynamic parameters in the look-up tables of the DASMAT simulation model. The original values of these parameters and their changed values after damage are listed in Table 1.

Table 1 The values of aerodynamic coefficients before and after 50% tip loss of rudder

	$C_{n\beta}$	$C_{n_{\delta_r}}$	C_{n_r}
original value	0.153	-0.1	-0.21
value after damage	0.122	-0.05	-0.168

In the simulation shown in Fig. 6, the rudder damage is triggered at $15s$. An impulse of external yaw moment ΔC_n is added at $15s$ and lasts for 2 seconds to simulate the effect of disturbances and turbulence, which causes an immediate rise of the averaged errors of C_n. As shown in Fig. 6(a), $\bar{\Delta} C_n$ exceeds the triggering threshold (3×10^{-7}) twice. Under the influence of an external yaw moment, β deviates from zero (Fig. 6(b)) and the rudder immediately

deflects in response to the sudden change (Fig. 6(c)), which excites the identification of C_{n_β} and $C_{n_{\delta_r}}$ respectively. In Figs. 6(e)(f), the value of C_{n_β} changes from 0.147 to 0.12, and $C_{n_{\delta_r}}$ from -0.095 to -0.046. It can be observed from Fig. 6(d) that even though both parameters converge to their changed values, the variance of C_{n_β} converges a bit slower than that of $C_{n_{\delta_r}}$. This is due to different excitation inputs of β and δ_r.

In the damage assessment system, each classifier corresponds to one damage case, and the output of each classifier is represented by an indication flag with the value of 0 or 1 . Whichever flag becomes unity, its corresponding damage case is declared as the current damage case. In this simulation, the assessment system requires at least 50 converged samples to generate the classification flag, which is $0.5s$ if the sampling rate is 100Hz. Based on the identification results shown on the left axis, the flags of the expected damage case are shown on the right axis of Figs. 6(e)(f).

It can be observed from Fig. 6 that the system is fully excited by large external yaw moments so that no further maneuvers are needed to get the desired results. In the simulation shown in Fig. 7, the amplitude of the added impulse signal is reduced in order to simulate the situation where the re-stabilizing response of β is not enough to fully excite the identification of C_{n_β}. As shown in Fig. 7(b)(c), at the time of damage occurrence, β deviates from zero and the controller gives commands of δ_r to maintain zero sideslip angle, which generates the excitation inputs to the re-identification of C_{n_β} and $C_{n_{\delta_r}}$. Fig. 7(d) shows that before $20s$, the variance of the estimated C_{n_β} did not converge to a small value as that of $C_{n_{\delta_r}}$, since the excitation of β is not sufficient.

From the perspective of identification, more β-maneuvers are required for more accurate result, but this may also increase the risk of LOC in the current abnormal situation that has not yet been fully identified. Safety is always the first priority when it comes to flight, so small maneuvers are suggested when giving excitation inputs. However, the criteria for "small" are hard to define. In this simulation, a limit of $\pm 2^\circ$ for β is suggested for the range of beta-maneuvers. The limit is based on the flight envelope of the most severe but still recoverable rudder-damage case retrieved from the database, in order to prevent the aircraft from entering the LOC condition during the identification process.

As shown in Fig. 7, starting at $20s$ a series of β-command is manually given within the limits, which provides more excitation for the estimated C_{n_β} to approach its expected value around $25s$. It can be observed that under damage conditions, the uncertainty in the identification is magnified due to limited range of maneuvers and the insufficiency of excitation.

Since the estimated variance provides a convenient metric for assessing whether C_{n_β} can be adequately identified, decision will be made based on the value of its variance of estimation. If the variance is under a certain threshold, it means that the estimation is close to the expected value. Given the high generalization ability of pattern classification, even an moderately accurate C_{n_β} can still generate the expected classification results, as shown in Fig. 7(e). If the variance of estimation remains at a value above the threshold, it means that the estimated C_{n_β} deviates too far from the expected value, and can not be included as a feature input in the classification. Under this condition, the classification will only depend on the identification of $C_{n_{\delta_r}}$, which converges more easily since rudder deflections δ_r in the inner loop have faster dynamics and thus generate sufficient excitation.

The comparison between flights with and without updated β-protection after rudder damage is shown in Fig. 8. Before damage occurs, the sideslip angle β is maintained at around -5°. The deflection of rudder experienced an increase at the time of damage ($15s$), which is necessary to maintain the same value of β and generates the errors shown in Fig. 8(a). Based on the identified $C_{n_{\delta_r}}$, rudder damaged is quickly classified and confirmed after the damage. As shown in Figs. 8(b)(c), at $20s$ the reference input for β continues to increase until the damaged rudder begins to saturate. It is observed from Fig. 8(b) that excessive β-commands are given because of the lack of the information on the new limit, so that the aircraft is under the protection of a static envelope. Due to actuator saturation shown in Fig. 8(c), the directional control in Fig. 8(b) is not regained until after $42s$, which is more than 10 seconds after the β-command is reduced at $30s$. Even though saturation did not cause the aircraft to flip over, strong forces at extreme positions may trigger more severe damage, like the total loss of rudder and vertical stabilizer. In addition, control effector saturation by itself can be a precursor to LOC, which means it should be avoided at all times. With updated information of the changed envelope shown in Fig. 4(a), the same excessive input command is limited within the bounds of the online updated envelope, as shown in Figs. 8(e)(f), which makes sure that the rudder deflections are always kept within the saturation limit.

B. Left Wing and Aileron Damage

Unlike rudder damage, wing damage is asymmetrical, generating an incremental rolling moment ΔC_l from unequal lift force (ΔC_{l_L}) and weight (ΔC_{l_W}) of two wing spans, as shown in the lower right subplot of Fig. 3. Since the reduction of weight is much less compared to lift force, its contribution to ΔC_l is neglected.

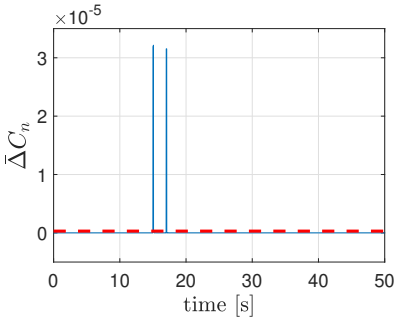

(a) Re-identification is triggered after the damage by a threshold: 3×10^{-7} (red dotted line)

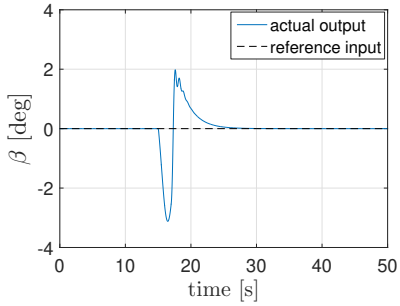

(b) Yaw responses to the damage and external yaw moments

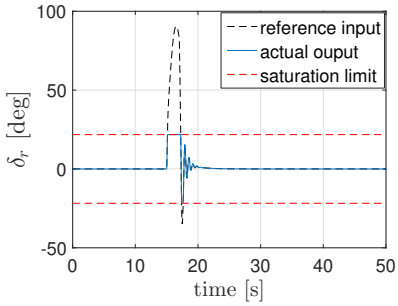

(c) Rudder control input and output after the damage

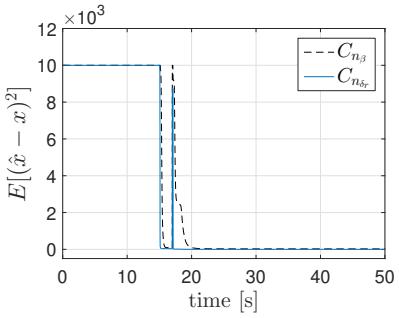

(d) The variances of re-identified aerodynamic coefficients converge after the damage

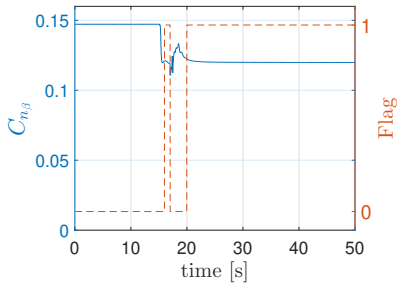

(e) The identified value of C_{n_β}(left) and the corresponding damage flag from classification (right)

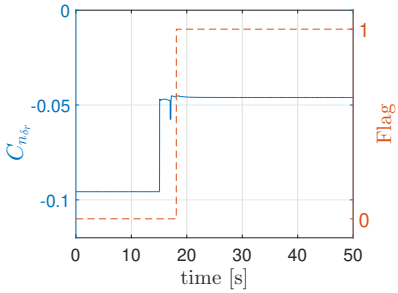

(f) The identified value of $C_{n_{\delta_r}}$ (left) and the corresponding damage flag from classification (right)

Fig. 6 The online identification and classification results of the rudder damage when the system is fully excited by large external yaw moments so that no further maneuvers are needed

Figure 9 shows data from NASA wind-tunnel experiments conducted on a generic fixed-wing aircraft model [9], which indicates how incremental rolling moments change with angle of attack under wing damage. It is observed that ΔC_l can be approximated by a linear function of α in low-angle-of-attack regions between $\alpha = -5°$ and $\alpha = 10°$. Hence, ΔC_l in DASMAT can be modeled as:

$$\Delta C_l = C_{l_\alpha} \cdot \alpha \tag{14}$$

As indicated by the wind-tunnel tests [9], the damage also induces reduction in the stability and control authority of the aircraft, which is reflected in the changed values of aerodynamic coefficients like the control effectiveness $C_{l_{\delta_a}}$ and roll damping C_{l_p}. The changes of C_{l_α}, $C_{l_{\delta_a}}$ and C_{l_p} are modeled in the DASMAT to simulate the influence of the damage. In this example, a damage case of 50% tip loss of left wing is simulated. Table 2 lists the original values of these significantly influenced coefficients in the look-up table and their modeled values after damage.

Table 2 The values of aerodynamic coefficients before and after 50% tip loss of left wing

	C_{l_p}	$C_{l_{\delta_a}}$	C_{l_α}
original value	-0.46	-0.186	0
value after damage	-0.345	-0.093	0.6

Similar to the rudder damage, the classification training is also based on two features, which are $C_{l_{\delta_a}}$ and C_{l_p}. It should be noted that even though C_{l_α} also changes after damage, it is not necessarily included as a classification feature, since the re-identification of this parameter may require large maneuvers of α to get sufficient inputs, which poses potential risk to the damaged aircraft. Figure 10 shows the training result of three different levels of wing damage to be used in the classification.

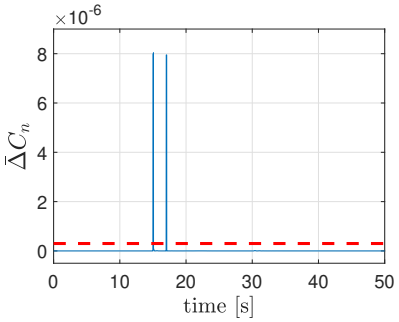

(a) Re-identification is triggered after the damage by a threshold: 3×10^{-7} (red dotted line)

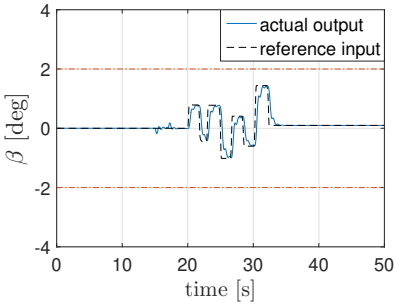

(b) Yaw responses to the damage and further maneuvers initiated after 20s

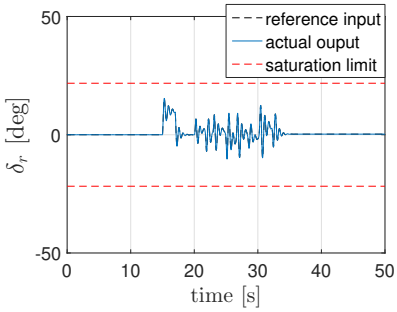

(c) Rudder control input and output after the damage

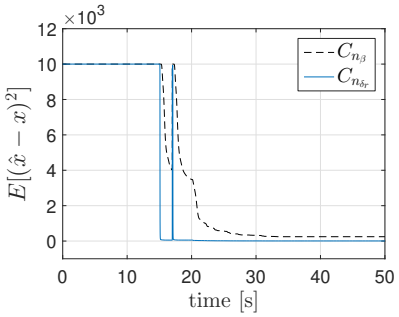

(d) The variances of re-identified aerodynamic coefficients converge after the damage

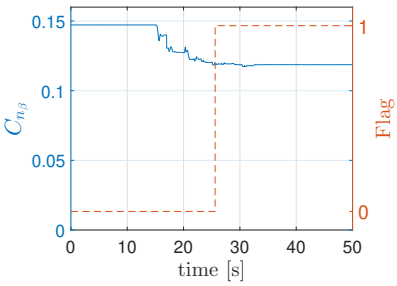

(e) The identified value of C_{n_β}(left) and the corresponding damage flag from classification (right)

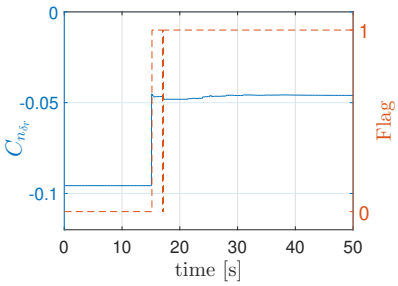

(f) The identified value of $C_{n_{\delta_r}}$ (left) and the corresponding damage flag from classification (right)

Fig. 7 The online identification and classification results of the rudder damage when the system is not fully excited by small external yaw moments so that further maneuvers are initiated

As shown in Fig. 11(a), the damage is initiated at 5s, and the averaged errors of the incremental rolling moment $\overline{\Delta}C_l$ suddenly increases above the threshold, which triggers the re-identification. Sufficient excitation for identification is less of an issue compared to rudder damage due to the existence of the incremental moment. In response to the sudden roll motion at 5s (Fig. 11(b)), the undamaged (right) aileron deflects in an effort to re-trim the aircraft and compensate for the incremental moment ΔC_l, as shown in Fig. 11(c). Meanwhile, the aileron deflections and roll motions have provided sufficient excitation inputs to the re-identification of aerodynamic coefficients, as can be observed from the variance convergence in Fig. 11(d). The identified C_{l_p}, $C_{l_{\delta_a}}$ are shown on the left axis of Figs. 11(e)(f) and the classification results on the right.

As shown in Figs. 11(b)(c), in the course of re-stabilizing the aircraft, the aileron needs to deflect about 25° to keep the roll angle at zero, leaving limited authority (13°) for further roll control. If ΔC_l continues to increase, the right aileron will saturate and the aircraft may enter into LOC if velocity does not increase within a short period of time.

According to the previous analysis of wing damage and Eq. 14, the increase of α may generate too much rolling moment saturating the actuator and leading to uncontrollable roll motions. Under normal conditions without damage, as shown in Fig. 12(a), the angle of attack can be controlled to increase to above 8° during pitch maneuvers, and the roll motion is barely influenced (Fig. 12(d)) due to decoupled effect of α. In the wing damage scenario shown in Fig. 12(b), the command of α starts to increase at 30s after the damaged aircraft has been re-trimmed. Under the coupled influence of wing damage, the value of aileron deflection δ_a increases with α (Fig. 12(e)) to compensate for the rolling moment. As shown in Figs. 12(b)(e), α increases to about 5.5° when δ_a meets the upper limit and the aircraft starts rolling to one side under the incremental rolling moment that can not be counteracted. This indicates that the protection of static flight envelopes no longer works and the angle of attack needs to be controlled within the updated envelope, so that the damaged aircraft is not subjected to an uncontrollable rolling moment.

The flight under envelope protection is shown in the right column of Fig. 12, where the updated envelope is retrieved based on the current damage case and flight states (see Fig. 4(b)). The reference input of α given by pilots/autopilot is not directly sent to the controller, but restricted by the retrieved envelope to about 5.2° before the deflection of δ_a

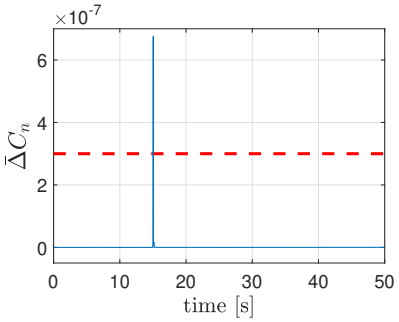

(a) Re-identification is triggered after the damage by a threshold: 3×10^{-7} (red dotted line)

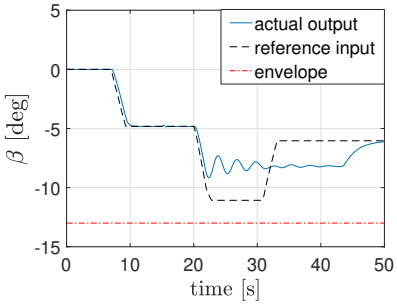

(b) The protection of a static envelope is not effective and the β control is lost after the damage

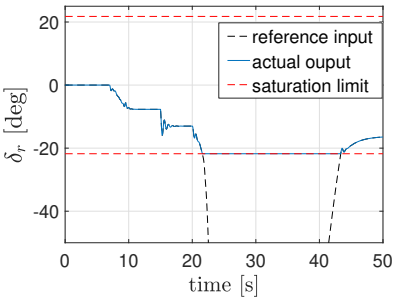

(c) The rudder is saturated under the protection of a fixed envelope after the damage

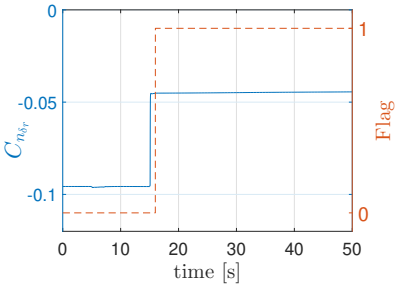

(d) The identified value of $C_{n_{\delta_r}}$ (left) and the corresponding damage flag from classification (right)

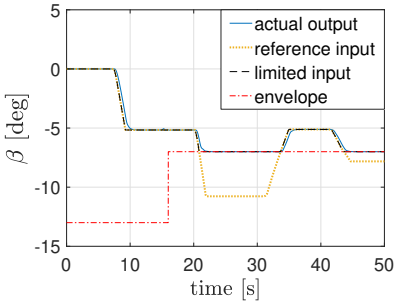

(e) The β-maneuver is under control with the protection of an updated envelope after the damage

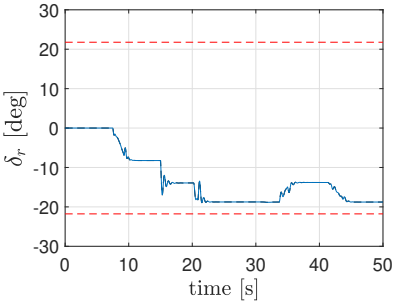

(f) The rudder is within the saturation limit under the protection of an updated envelope after the damage

Fig. 8 Comparisons of β control between static and online updated flight envelope protection after 50% tip loss of rudder

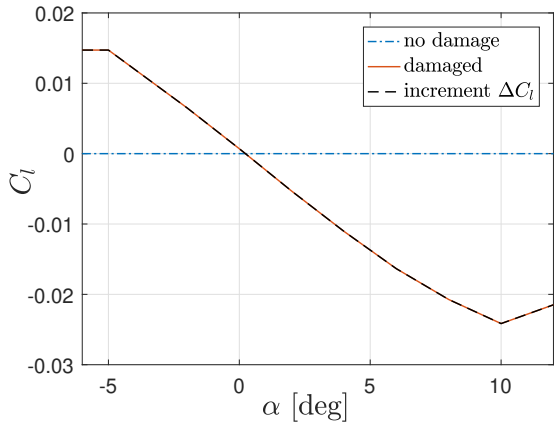

(a) $\beta = 0$

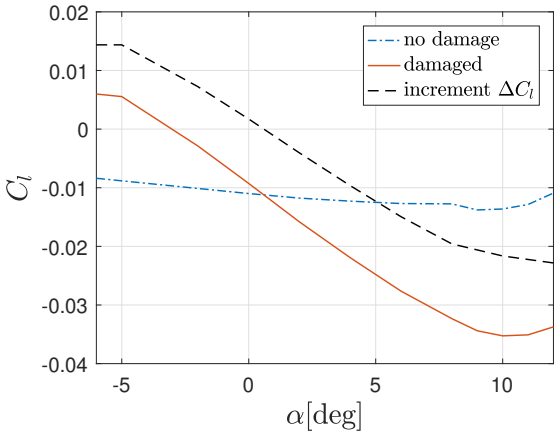

(b) $\beta = 5°$

Fig. 9 Wind-tunnel data of incremental rolling moment with respect to angle of attack

is computed by the INDI controller. As shown in Fig. 12(f), δ_a is kept within the limit so that there is no unwanted rolling motion during pitching maneuvers and the damaged aircraft is always under control.

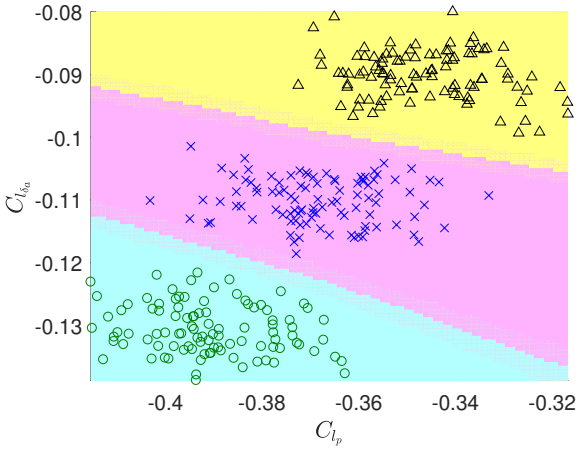

Fig. 10 Training result of wing damage using neural networks (damage levels ◯ : 30% × : 40% Δ : 50%)

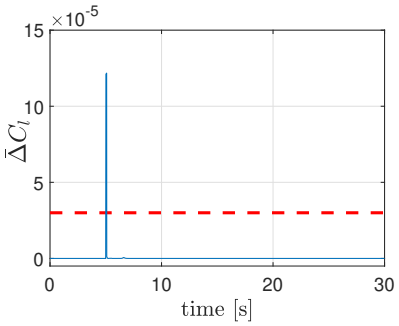

(a) Re-identification is triggered after the damage by a threshold: 3×10^{-5} (red dotted line)

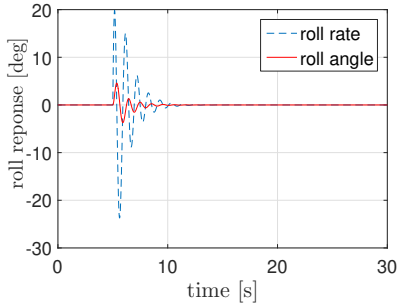

(b) Roll responses to the damage and incremental rolling moments

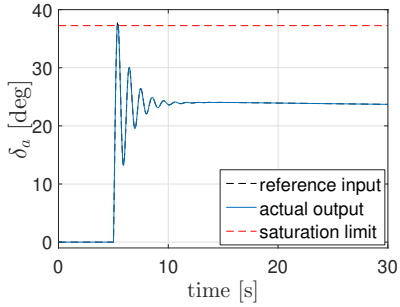

(c) Aileron control input and output after the damage

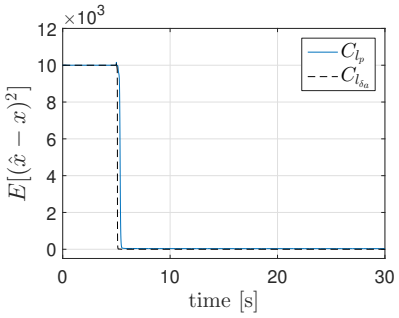

(d) The variances of re-identified aerodynamic coefficients converge after the damage

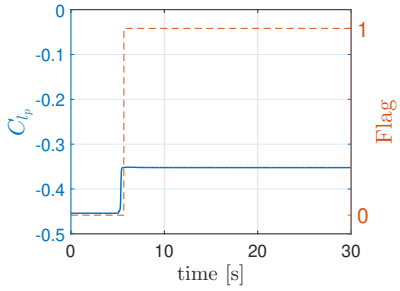

(e) The identified value of C_{l_p} (left) and the corresponding damage flag from classification (right)

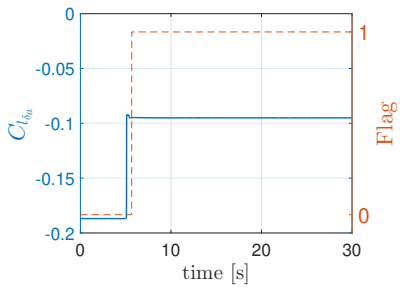

(f) The identified value of $C_{l_{\delta_a}}$ (left) and the corresponding damage flag from classification (right)

Fig. 11 The online identification and classification results of the wing damage

C. Combined Rudder and Wing Damage

In this example, both the left wing and the rudder are damaged at 5s and 15s respectively, which result in combined aerodynamic effect on the aircraft where the updated envelopes of both α and β are needed.

In the simulation shown in Fig. 13(a), the aircraft is under well-protection after the wing damage occurs at 5s with the updated flight envelope. However, the situation of wing damage deteriorates after the occurrence of rudder damage, and the single α-envelope protection is no longer effective.

In case of single damage of rudder, as previously shown in Fig. 8(b), the saturation will cause deviations from the

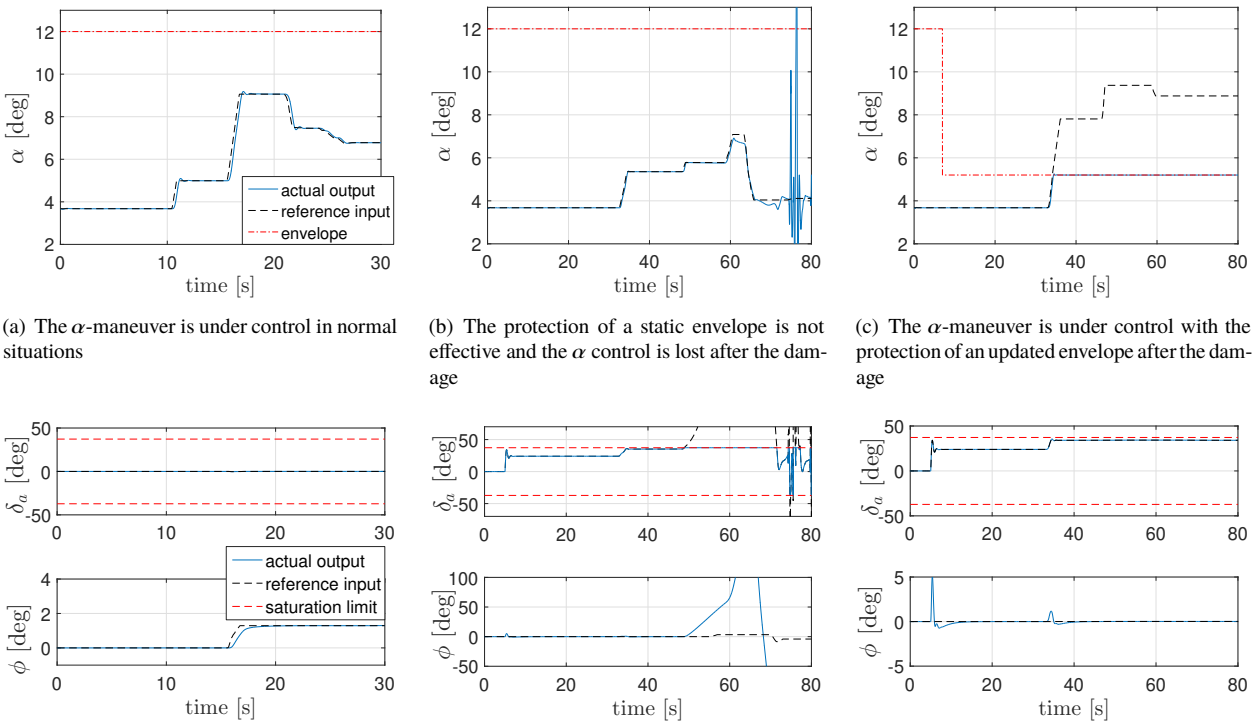

(a) The α-maneuver is under control in normal situations

(b) The protection of a static envelope is not effective and the α control is lost after the damage

(c) The α-maneuver is under control with the protection of an updated envelope after the damage

(d) The aileron deflections and roll responses in normal situations

(e) The aileron deflections and roll responses in the loss-of-control condition

(f) The aileron deflections and roll responses under effective flight envelope protection

Fig. 12 Comparisons of α control between static and online updated flight envelope protection after 50% wing tip loss

commanded β, but not total LOC of the aircraft. However, when rudder damage is combined with wing damage, the envelope protection of β becomes critical, due to the coupling between directional and lateral motions.

As shown in Fig. 13(b), after the rudder is damaged at 15s, the flight envelope is not updated and the increasing command of β is not limited. At around 20s, the control of β is lost without effective β-envelope protection and the rudder is saturated (Fig. 13(c)). Due to the typically large effective dihedral (C_{l_β}) of swept-wing transport aircraft, the uncontrolled yaw motion generates more rolling moments that require additional aileron deflections. Meanwhile, in the extreme situation shown in Fig. 13(a), the α-command has gone beyond the safe limit and the actual α is maintained within the envelope boundary and the aileron deflection is at the edge of saturation before 20s. Therefore, when both ailerons and rudder are saturated, the additional rolling moment cannot be mitigated by the remaining control authorities, which causes the aircraft to roll to one side and become unrecoverable.

It can be concluded that the protection of α can no longer prevent the aircraft from LOC if β is not effectively protected in the situation of combined damage. As shown in the second row of Fig. 13, the utilization of both β and α envelope protection can effectively prevent a LOC situation when, for example, pilots give excessive commands to the controller under emergencies. The flight envelope of the combined damage, as shown in Fig. 4(c), is stored in the database and retrieved to replace and update the normal static envelope once the damage is identified.

D. Discussion

To test the reliability of the system, 300 simulation flights were conducted under structural damage of different settings such as damage locations, damage levels, initial conditions and excitation scales etc. It is recorded that during 287 (95.6%) flights the system was able to correctly identify and classify the damage case within 10 seconds in simulation time, and all these flights were successfully prevented from LOC by the envelope protection strategy proposed in this paper. It is found that the more severe the damage case is, the quicker the case can be detected and identified. Due to the existence of noise and disturbances, the system failed to detect 13 flights under slight damage, which, however, did not trigger LOC under the protection of normal envelopes.

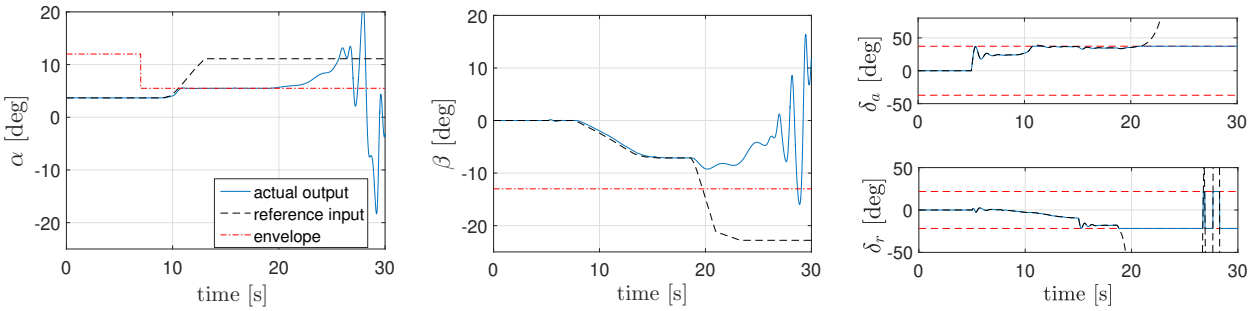

(a) The α-control is lost without effective envelope protection

(b) The β-control is lost without effective envelope protection

(c) Both the ailerons and rudder become saturated under the LOC condition

(d) The α-control is effectively protected with updated flight envelopes of α and β

(e) The β-control is effectively protected with updated flight envelopes of α and β

(f) Under the protection of both α and β envelopes, the damaged actuators are prevented from saturation

Fig. 13 In the situation of combined damage, the aircraft can be prevented from LOC only if both α and β envelopes are updated and protected

Among all the LOC hazards that have a fundamental influence on flight envelopes, structural damage discussed in this paper is only one category. Combination with other abnormal cases can lead to further changes of flight envelopes and more stringent protection strategies. For example, icing-induced LOC incidents and accidents have occurred on all classes of aircraft [13, 27]. The primary aerodynamic effect of icing is the increased drag force and reduced lift force on the icing part. Normally ice accretion is not symmetrical, thus inducing moments from unequal forces. Based on this analysis, icing can be regarded as a modification of the airframe outline, and its aerodynamic impact is similar to that of structural damage discussed in this paper. Due to the lack of aerodynamic modeling data, icing is not modeled and simulated in this paper. In future work, the flight envelope protection system can be augmented to include more abnormal cases like icing with more experimental data and high-fidelity models.

It should also be noted that the cooperation between pilots and the automatic controller plays a vital role in some complicated situations like engine failures and actuator faults [12, 28]. The identification and classification approach used in this paper can also be used to retrieve envelopes for use of pilot warning and flight display to enhance the situational awareness of the pilots. Therefore, future improvement work can be focused on the integration of human-machine interactions into the flight envelope protection system proposed in this paper.

V. Conclusion

A flight envelope protection system with online-updated envelope information is developed in this paper. The system is implemented online in closed loop, combining fault tolerant flight control, system identification, damage assessment and database retrieval. Three in-flight damage cases are conducted in the simulation to test the performance of the flight envelope protection system. In addition, practical issues about insufficient excitation for system identification under damage are addressed in the simulation. The test results show a success rate of 95.6% of 300 simulated flights under different damage cases and maneuver conditions, which indicates that the proposed system can be implemented online and effectively help prevent the damaged aircraft from flying into loss-of-control conditions.

References

[1] Tekles, N., Chongvisal, J., Xargay, E., Choe, R., Talleur, D. A., Hovakimyan, N., and Belcastro, C. M., "Design of a Flight Envelope Protection System for NASA's Transport Class Model," *Journal of Guidance, Control, and Dynamics*, Vol. 40, No. 4, 2017, pp. 863–877. doi:10.2514/1.G001728, URL https://arc.aiaa.org/doi/10.2514/1.G001728.

[2] Lee, H., Snyder, S., and Hovakimyan, N., "L1 Adaptive Control Within a Flight Envelope Protection System," *Journal of Guidance, Control, and Dynamics*, Vol. 40, No. 4, 2017, pp. 1013–1026. doi:10.2514/1.G001742, URL https://arc.aiaa.org/doi/10.2514/1.G001742.

[3] Briere, D., and Traverse, P., "AIRBUS A320/A330/A340 Electrical Flight Controls - A Family of Fault-tolerant Systems," *FTCS-23 The Twenty-Third International Symposium on Fault-Tolerant Computing*, 1993, pp. 616–623. doi:10.1109/FTCS.1993.627364, URL http://ieeexplore.ieee.org/document/627364/.

[4] Falkena, W., Borst, C., Chu, Q., and Mulder, J., "Investigation of Practical Flight Envelope Protection Systems for Small Aircraft," *Journal of Guidance, Control, and Dynamics*, Vol. 34, No. 4, 2011, pp. 976–988. doi:10.2514/1.53000, URL http://arc.aiaa.org/doi/10.2514/1.53000.

[5] Ackerman, K. A., Talleur, D. A., Carbonari, R. S., Xargay, E., Seefeldt, B. D., Kirlik, A., Hovakimyan, N., and Trujillo, A. C., "Automation Situation Awareness Display for a Flight Envelope Protection System," *Journal of Guidance, Control, and Dynamics*, Vol. 40, No. 4, 2017, pp. 964–980. doi:10.2514/1.G000338, URL https://arc.aiaa.org/doi/10.2514/1.G000338.

[6] Lombaerts, T. J. J., Looye, G., Ellerbroek, J., and Martin, M. R. y., "Design and Piloted Simulator Evaluation of Adaptive Safe Flight Envelope Protection Algorithm," *Journal of Guidance, Control, and Dynamics*, Vol. 40, No. 8, 2017, pp. 1902–1924. doi:10.2514/1.G002525, URL https://arc.aiaa.org/doi/pdf/10.2514/1.G002525.

[7] Van Baelen, D., Ellerbroek, J., van Paassen, M. M., and Mulder, M., "Design of a Haptic Feedback System for Flight Envelope Protection," *AIAA Modeling and Simulation Technologies Conference*, 2018. doi:10.2514/6.2018-0117, URL https://arc.aiaa.org/doi/10.2514/6.2018-0117.

[8] Ellerbroek, J., Martin, M. J., Lombaerts, T. J. J., van Paassen, M. M., and Mulder, M., "Design and evaluation of a Flight Envelope Protection haptic feedback system," *IFAC-PapersOnLine*, Vol. 49, No. 19, 2016, pp. 171–176. doi:10.1016/j.ifacol.2016.10.481, URL http://dx.doi.org/10.1016/j.ifacol.2016.10.481.

[9] Shah, G. H., "Aerodynamic Effects and Modeling of Damage to Transport Aircraft," *AIAA Guidance, Navigation and Control Conference and Exhibit*, 2008. URL http://arc.aiaa.org/doi/pdf/10.2514/6.2008-6203.

[10] Zhang, Y., de Visser, C. C., and Chu, Q. P., "Aircraft Damage Identification and Classification for Database-Driven Online Flight-Envelope Prediction," *Journal of Guidance, Control, and Dynamics*, Vol. 41, No. 2, 2018, pp. 449–460. doi:10.2514/1.G002866, URL https://arc.aiaa.org/doi/10.2514/1.G002866.

[11] Zhang, Y., de Visser, C. C., and Chu, Q. P., "Database Building and Interpolation for an Online Safe Flight Envelope Prediction System," *Journal of Guidance, Control, and Dynamics*, 2019, pp. 1–9. doi:10.2514/1.G003834.

[12] Koolstra, H., "Preventing Loss of Aircraft Control: Aiding pilots in manual recovery from roll-limited situations," Ph.D. thesis, Delft University of Technology, 2017.

[13] Gingras, D., Ranaudo, R., Barnhart, B., Ratvasky, T., and Morelli, E., "Envelope Protection for In-Flight Ice Contamination," *AIAA Aerospace Sciences Meeting*, 2009. doi:10.2514/6.2009-1458, URL http://arc.aiaa.org/doi/10.2514/6.2009-1458.

[14] Patton, R. J., "Fault-Tolerant Control: The 1997 Situation," *Proc. of the IFAC Symp. SAFEPROCESS 97*, Kingston Upon Hull, UK, 1997, pp. 1033–1055. doi:10.1016/S1474-6670(17)42536-5.

[15] Zhang, Y., and Jiang, J., "Bibliographical review on reconfigurable fault-tolerant control systems," *Annual Reviews in Control*, Vol. 32, No. 2, 2008, pp. 229–252. doi:10.1016/j.arcontrol.2008.03.008.

[16] Bacon, B., Ostroff, A. J., and Joshi, S., "Reconfigurable NDI Controller Using Inertial Sensor Failure Detection & Isolation," *Aerospace and Electronic Systems, IEEE Transactions on*, Vol. 37, No. 4, 2001, pp. 1373–1383. doi:10.1109/7.976972.

[17] Sieberling, S., Chu, Q. P., and Mulder, J. A., "Robust Flight Control Using Incremental Nonlinear Dynamic Inversion and Angular Acceleration Prediction," *Journal of Guidance, Control, and Dynamics*, Vol. 33, No. 6, 2010, pp. 1732–1742. doi:10.2514/1.49978, URL http://arc.aiaa.org/doi/10.2514/1.49978.

[18] Lombaerts, T., Huisman, H., Chu, P., Mulder, J. A., and Joosten, D., "Nonlinear Reconfiguring Flight Control Based on Online Physical Model Identification," *Journal of Guidance, Control, and Dynamics*, Vol. 32, No. 3, 2009, pp. 727–748. doi:10.2514/1.40788, URL http://arc.aiaa.org/doi/10.2514/1.40788.

[19] Tol, H. J., Visser, C. C. D., Sun, L. G., Kampen, E. V., and Chu, Q. P., "Multivariate Spline-Based Adaptive Control of High-Performance Aircraft with Aerodynamic Uncertainties," *Journal of Guidance, Control, and Dynamics*, Vol. 39, No. 4, 2016, pp. 781–800. doi:10.2514/1.G001079.

[20] Smeur, E. J. J., Chu, Q., and de Croon, G. C. H. E., "Adaptive Incremental Nonlinear Dynamic Inversion for Attitude Control of Micro Air Vehicles," *Journal of Guidance, Control, and Dynamics*, Vol. 39, No. 3, 2016, pp. 450–461. doi:10.2514/1.G001490, URL http://arc.aiaa.org/doi/10.2514/1.G001490.

[21] Sun, S., Sijbers, L., Wang, X., and de Visser, C. C., "High-Speed Flight of Quadrotor Despite Loss of Single Rotor," *IEEE Robotics and Automation Letters*, Vol. 3, No. 4, 2018, pp. 3201–3207. doi:10.1109/LRA.2018.2851028.

[22] Simplício, P., Pavel, M. D., van Kampen, E., and Chu, Q. P., "An acceleration measurements-based approach for helicopter nonlinear flight control using incremental nonlinear dynamic inversion," *Control Engineering Practice*, Vol. 21, No. 8, 2013, pp. 1065–1077. doi:10.1016/j.conengprac.2013.03.009, URL http://dx.doi.org/10.1016/j.conengprac.2013.03.009.

[23] Matamoros, I., and de Visser, C. C., "Incremental Nonlinear Control Allocation for a Tailless Aircraft with Innovative Control Effectors," *AIAA Guidance, Navigation, and Control Conference*, 2018. doi:10.2514/6.2018-1116, URL https://arc.aiaa.org/doi/10.2514/6.2018-1116.

[24] Lu, P., van Kampen, E. J., de Visser, C., and Chu, Q., "Aircraft fault-tolerant trajectory control using Incremental Nonlinear Dynamic Inversion," *Control Engineering Practice*, Vol. 57, 2016, pp. 126–141. doi:10.1016/j.conengprac.2016.09.010, URL http://dx.doi.org/10.1016/j.conengprac.2016.09.010.

[25] Grondman, F., Looye, G., Kuchar, R. O., Chu, Q. P., and Van Kampen, E.-J., "Design and Flight Testing of Incremental Nonlinear Dynamic Inversion-based Control Laws for a Passenger Aircraft," *2018 AIAA Guidance, Navigation, and Control Conference*, 2018. doi:10.2514/6.2018-0385, URL https://arc.aiaa.org/doi/10.2514/6.2018-0385.

[26] Van Der Linden, C. A. A. M., *DASMAT-Delft University Aircraft Simulation Model and Analysis Tool: A Matlab/Simulink Environment for Flight Dynamics and Control Analysis.*, Delft University of Technology, 1996.

[27] Lombaerts, T., Looye, G., Seefried, A., Neves, M., and Bellmann, T., "Proof of concept simulator demonstration of a physics based self-preserving flight envelope protection algorithm," *Engineering Applications of Artificial Intelligence*, Vol. 67, No. August 2017, 2018, pp. 368–380. doi:10.1016/j.engappai.2017.08.014, URL http://dx.doi.org/10.1016/j.engappai.2017.08.014.

[28] Di Donato, P. F. A., Balachandran, S., McDonough, K., Atkins, E. M., and Kolmanovsky, I., "Envelope-Aware Flight Management for Loss of Control Prevention Given Rudder Jam," *Journal of Guidance, Control, and Dynamics*, Vol. 40, No. 4, 2017, pp. 1027–1041. doi:10.2514/1.G000252, URL https://arc.aiaa.org/doi/10.2514/1.G000252.